Adsorption capacity of the corrosion products of nanoscale zerovalent iron towards emerging contaminants

Junmin Deng, Sungjun Bae, Sunho Yoon, Mathieu Pasturel, Remi Marsac, Khalil Hanna

View Article Online
View Journal

Environmental Science Nano

Accepted Manuscript

This article can be cited before page numbers have been issued, to do this please use: J. Deng, S. Bae, S. Yoon, M. Pasturel, R. Marsac and K. Hanna, *Environ. Sci.: Nano*, 2020, DOI: 10.1039/D0EN00886A.

ROYAL SOCIETY OF CHEMISTRY

rsc.li/es-nano

Environmental Significance Statement

Although the large variety of applications of nanoscale zero-valent iron (NZVI) on environmental remediation, little is known about the reactivity and the fate of the NZVI passivation products which continue to migrate in natural systems. This work shows for the first time how the corrosion products of NZVI could bind co-exiting contaminants (e.g. antibiotics), and then affect their fate in natural systems. Spectroscopic and microscopic investigations revealed a gradual increase in Fe(II) content at the surface of secondary Fe minerals over the passivation time. Formation of surface bound Fe(II) enhanced adsorption of emerging contaminants onto the secondary magnetite phase, which is also pH dependent. A surface complexation model is then proposed to account for the impact of Fe(II) content on the adsorption behavior into secondary Fe minerals. This work sheds light on an overseen aspect of the reactivity of secondary minerals resulting from NZVI corrosion, which should be considered in fate and transport modeling of contaminants.

View Article Online
DOI: 10.1039/D0EN00886A

Adsorption capacity of the corrosion products of nanoscale zerovalent iron towards emerging contaminants

Junmin Deng[1,2], Sungjun Bae[2], Sunho Yoon[2], Mathieu Pasturel[3], Rémi Marsac[4], Khalil Hanna[1,5*]

[1] *Univ. Rennes, Ecole Nationale Supérieure de Chimie de Rennes, CNRS, ISCR-UMR 6226, F-35000, Rennes, France*

[2] *Department of Civil and Environmental Engineering, Konkuk University, 120 Neungdong-ro, Gwangjin-gu, Seoul 05029, Republic of Korea*

[3] *Univ. Rennes, CNRS, ISCR – UMR 6226, F-35000, Rennes, France*

[4] *Univ. Rennes, CNRS, Géosciences Rennes – UMR 6118, F-35000 Rennes, France*

[5] *Institut Universitaire de France (IUF), MESRI, 1 rue Descartes, 75231 Paris, France*

*Corresponding author: khalil.hanna@ensc-rennes.fr

A revised manuscript to *Environmental Science: Nano*

October 2020

View Article Online
DOI: 10.1039/D0EN00886A

Abstract

Despite the extensive use of nanoscale zerovalent iron (NZVI) in water and soil remediation, no data exist on the reactivity of secondary iron minerals formed upon the NZVI corrosion. Herein, we investigated the oxidation kinetics of NZVI by monitoring the variations of pH, oxidation−reduction potential (ORP) and dissolved Fe(II) concentration, and then examined the reactivity of resulting oxidized particles for the adsorption of an emerging contaminant (nalidixic acid (NA)). NA adsorption was found greatest onto oxidized particles and negligible on the fresh NZVI. Interestingly, the formed secondary mineral phases exhibited an unusual pH adsorption-curve with an unexpected great adsorption at alkaline pH values. X-ray photoelectron spectroscopy and high resolution-transmission electron microscopy revealed a gradual increase in Fe(II) content at the surface of magnetite phase over the reaction time. Additional experiments and surface complexation modeling showed that the enhanced adsorption of NA onto the secondary magnetite is due to the formation of surface bound Fe(II). Fe(II) release into solution because, for instance, of the presence of organic buffer molecules, decreased surface Fe(II) and then NA adsorption at alkaline pH values. This work sheds light on an overseen aspect of the reactivity of secondary iron minerals resulting from NZVI passivation, which can bind co-exiting emerging contaminants and then affect their fate in the environment.

View Article Online
DOI: 10.1039/D0EN00886A

1. Introduction

Because nanoscale zerovalent iron (NZVI) is an environmentally-safe material and exhibits great particle reactivity, it has been widely used in treatment processes of various organic and inorganic contaminants [1-3]. As a result, NZVI has become one of the most extensively studied nanomaterials in wastewater treatment and remediation of soil and groundwater.[4-7]

For the remediation action, the NZVI slurry is directly introduced into soil and groundwater systems, and NZVI particles migrate from the injection points to affected zones.[8] During this journey, NZVI could encounter many electron acceptors resulting in partial or complete oxidation of NZVI particles (also called surface passivation). These electron acceptors may include oxygen as in oxic environments, nitrate, etc. and targeted compounds, *i.e.* contaminants.[9-12] This oxidation can lead to either formation of Fe^{II}-bearing phases on the NZVI surface or complete oxidation to ferric (oxyhydr)oxides, depending upon various factors including type and concentration of co-existing species, reaction time and oxic/anoxic environments. For instance, lepidocrocite, magnetite and maghemite appeared to be the main secondary iron minerals formed upon the oxic corrosion of NZVI.[13]

Although the ability of NZVI to reductively transform a wide variety of compounds has been extensively investigated, little is known about the fate of injected NZVI particles in natural systems. In addition, NZVI passivation byproducts have been

View Article Online
DOI: 10.1039/D0EN00886A

identified under oxic and anoxic conditions,[14] but no data exist on the reactivity of these byproducts in nature. Indeed, the passivation byproducts (i.e., secondary Fe minerals) would continue to migrate in environmental settings and potentially meet other types of contaminants. They could bind co-existing contaminants and then influence their aqueous or colloidal transport in soil and groundwater. Comprehensive examination of the reactivity of these "abandoned" particles and their mobility in natural settings is essential for ecological risk assessments.

Here, we examined the interactions between NZVI (fresh or passivated) and nalidixic acid (NA), a quinolone antibiotic widely used in human and veterinary medicine. NA was selected as a target emerging contaminant because it has been frequently detected in the environment (at concentration levels ranging from $ng \cdot L^{-1}$ to $\mu g \cdot L^{-1}$).[15,16] To control the NZVI oxidation in aqueous suspension, hydrogen peroxide (H_2O_2) was used under anoxic conditions (N_2 glove box). pH and oxidation−reduction potential (ORP) values and dissolved Fe(II) concentration were measured throughout the reaction, and transformation of NZVI particles were monitored by X-ray diffraction, X-ray photoelectron spectroscopy and high resolution-transmission electron microscopy (HR-TEM) equipped with the selected area electron diffraction (SAED). Adsorption tests were performed after total depletion of H_2O_2 in order to prevent any contribution from Fenton-like oxidation (mass balance was also checked) in NA removal. NA adsorption onto the resulting oxidized NZVI particles was evaluated as a function of pH and NA concentration. A surface complexation model was used to

View Article Online
DOI: 10.1039/D0EN00886A

account for the impact of Fe(II) content on the NA adsorption into secondary Fe minerals.

2. Materials and methods

2.1. Chemicals and materials

Nalidixic acid (NA, ≥99.0%), sodium borohydride ($NaBH_4$, ≥99.0%), ferric chloride hexahydrate ($FeCl_3.6H_2O$, ≥99.0%), hydrogen peroxide solution (H_2O_2, 30%), ferrous chloride tetrahydrate ($FeCl_2 \cdot 4H_2O$, ≥99.0%), 1,10-phenanthroline (≥99.0%), acetic acid (≥99.5%), hydrochloric acid (HCl, 37%), sodium hydroxide (NaOH, ≥99.0%), glycerol (≥99.5%), tetracycline hydrochloride (TET, ≥99.0%), 4-morpholineethanesulfonic acid (MES, ≥99.5%), 4-(2-hydroxyethyl)piperazine-1-ethanesulfonic acid (HEPES, ≥99.5%), tris(hydroxymethyl)aminomethane (TRIZMA base, ≥99.9%) and Tris(hydroxymethyl)aminomethane hydrochloride (TRIZMA HCl, ≥99.5%) were all purchased from Sigma-Aldrich, France. Leonardite Humic Acid standard (LHA) was purchased from the International Humic Substances Society (IHSS). Maghemite (γ-Fe_2O_3) was purchased from Alfa Aesar, with a high purity (>99.0%). Magnetite (Fe_3O_4), hematite (α-Fe_2O_3) and lepidocrocite (γ-FeOOH) were synthesized as previously reported.[17] Acetonitrile (99.99%, Sigma) and acetic acid (99.7%, ACROS) were used for mobile phase of high-performance liquid chromatography (HPLC). NA stock solution (5 mM) and ferrous chloride stock solution (100 mM) were prepared with 0.1 M NaOH and 0.1M HCl, respectively. Glassware

was soaked in a 5% (v/v) HCl container for at least 48 h and rinsed before use. Unless specifically stated, all solutions were prepared with deoxgenated deionized water (DDIW, 18.2 MΩ·cm) prepared by purging with nitrogen (N_2, 99.99%) for 4 hours and stored in anaerobic chamber (JACOMEX).

2.2. Synthesis and characterization of NZVI

NZVI was synthesized following our previous work.[18] Briefly, 500 mL of sodium borohydride solution (0.9 M) was added dropwise into the 500 mL of ferric chloride hexahydrate solution (0.11 M) a fixed rate of 1 mL/min in anaerobic chamber. After finishing the synthesis, the precipitates in the suspension were separated by magnet, then washed 3 times with DDIW. The obtained NZVI was dried and stored inside the anaerobic chamber.

The oxidized particles were then analyzed by X-ray diffraction (XRD, D8, BRUKER). The oxidized NZVI suspensions were washed with DDIW for three times, and dried in a vacuum freeze drier (-52℃, 24 h). Then, the dried samples were transferred to sample holders and treated with 1:1 (v:v) glycerol solution to avoid the surface oxidation during the analysis of XRD.[19] X-ray photoelectron spectroscopy (XPS, Sigma Probe system, Thermo) analysis was performed for four different samples (i.e., pristine NZVI, NZVI after reaction with H_2O_2 (3, 15, and 18 h). We used the power source (Al Kα X-ray, 1486.7 eV) of 75 W and the C 1s peak at 285 eV as a reference for correction of surface charging effects. The morphological characterization

of different oxidized NZVIs were investigated by high resolution-transmission electron microscopy (HR-TEM, JEM-2100, JEOL) equipped with the selected area electron diffraction (SAED). The specific surface area of oxidized NZVIs was analyzed by multi-point N_2 adsorption isotherm (Micromeritics, USA). The average particle size and zeta potential of the oxidized NZVI particles were measured by Zetasizer MAS (Matec Applied Sciences).

2.3. Analytical methods

Batch experiments were conducted in 500 mL flasks in anaerobic chamber to avoid the effect of dissolved oxygen during the reaction. 0.1 g NZVI was transferred to the flask containing 500 mL DDIW with stirring at 600 rpm to prepare an initial NZVI dosage of 200 mg/L. A portable pH-ORP meter (HANNA, HI991003) was used to monitor the variations in pH and ORP during the oxidation and adsorption processes. After a steady state was reached for both pH and ORP, exact amounts (0.25, 0.5, 1, 2.5 or 5 mL) of H_2O_2 stock solution (1 M) were introduced into the suspensions to prepare different oxidized NZVIs by different H_2O_2 concentration at 0.5, 1, 2, 5 or 10 mM, respectively. After reaching the equilibrium of pH and ORP again, 1 mL of NA stock solution (5 mM) was transferred into the suspension to initiate the adsorption of NA (10 μM) by the oxidized NZVI. At the sampling times, 1 mL samples were taken from the suspension and filtered through a 0.2 μm filter (Whatman) for analysis of high-

View Article Online
DOI: 10.1039/D0EN00886A

performance liquid chromatography (HPLC). After finishing 2-h adsorption, desorption tests were carried out at pH 12 to check the mass balance of NA (Table S1).

Aqueous concentration of NA was determined using HPLC (Waters 600 Controller) equipped with a photodiode array detector operating at 258 nm (Waters 996) and a reversed-phase C18 column (250 mm × 4.6 mm i.d., 5 μm). The mobile phase was a mixture of acetonitrile/water (60/40 v/v) containing 0.1% formic acid. The flow rate of the mobile phase was set at 1 mL/min in isocratic mode.[20] The dissolved Fe(II) concentration was measured by a 1,10-phenanthroline method at a wavelength of 510 nm using an UV–vis spectrophotometer (U-3310, HITACHI).

The same procedure was used to investigate the oxidation of NZVI in buffered systems. A constant Good's buffer (MES, HEPES and TRIZMA) concentration of 10 mM was used to maintain the pH at 5.6, 7.0 and 9.0, respectively[21-22]. These buffers were introduced into the reactor together with NZVI (200 mg/L).

All experiments were performed in triplicates, and the data reported here were the average of three replicated experiments and error bars represent the relative standard deviation.

2.4. Surface Complexation Modeling

The NA removal in the NZVI suspension at different pH values were described using surface complexation modeling. The geochemical speciation code PHREEQC and the "minteq" database were used.[23] The pK_a of NA is 6.19 and the logarithm of the

View Article Online
DOI: 10.1039/D0EN00886A

formation constant of NA−Fe^{+}(aq) is 3.99.[24] The surface complexation models for magnetite are used, as previously reported, [25] and the protonation of Fe surface sites is formulated following a 2-pK_a approach (Eqs. (1) and (2)).

$$\equiv FeOH_2^+ \leftrightarrows \equiv FeOH + H^+; pKa_1 \quad (1)$$

$$\equiv FeOH \leftrightarrows \equiv FeO^- + H^+; pKa_2 \quad (2)$$

Charge-potential relationship was described according to the constant capacitance model (CCM), and the modeling parameters are presented in the supporting information (Table S2). Though the CCM is not available in PHREEQC (version 2), we have adapted parameters of the three plane model (TPM) implemented in PHREEQC in order to use the CCM, as previously reported.[26]

3. Results and discussion

3.1. NZVI oxidation in aqueous solution and NA removal

Variations in pH, ORP and dissolved Fe(II) concentration were monitored during i) the addition of NZVI in reactor, ii) the oxidation of NZVI by H_2O_2, and iii) the removal of NA by the resulting secondary particles (Figure 1). When NZVI was added in water (i.e., the first 2-h period), we observed an obvious increase in pH (from 6.9 to 8.9) and a decrease in ORP (from 81 to -748 mV), which can be attributed to generation

View Article Online
DOI: 10.1039/D0EN00886A

of OH^-, Fe^{2+}, and H_2 during the anaerobic corrosion of NZVI (Eq.(3)).[27]

$$Fe^0 + 2H_2O \rightarrow Fe^{2+} + 2OH^- + H_2 \quad (3)$$

After adding H_2O_2 into the NZVI suspension, the ORP value increased rapidly up to 241 mV due to the standard potential of H_2O_2/ H_2O (1.37 V)[28], while pH dropped to 7.8 which is ascribed to the oxidation and hydrolysis of released iron ions. In addition, the release of H^+ from H_2O_2 dissociation (pK_a of 11.6) presumably results in pH decrease.[29]

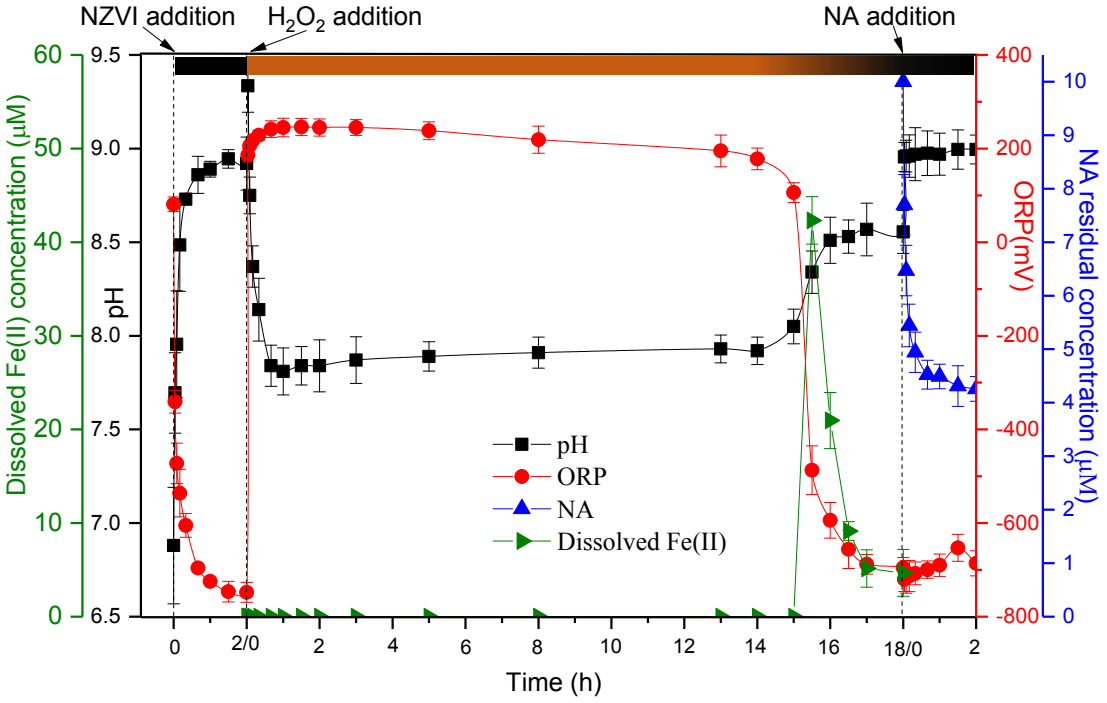

Figure 1. Variations in pH, ORP, color of suspension, dissolved Fe(II) concentration and NA concentration during the NZVI oxidation and NA adsorption. Experimental conditions: [NZVI] = 0.2 g·L^{-1}, $[H_2O_2]_{initial}$ = 5 mM, $[NA]_{initial}$ = 10 μM, 20 ±1 °C.

View Article Online
DOI: 10.1039/D0EN00886A

After a long steady-state period for both ORP and pH values (around 15 h), ORP decreased sharply until -696 mV and the pH increased to 8.6, which can be attributed to the complete consumption of H_2O_2 (as it is also verified by the molybdate-catalyzed iodometric titration method[30]). During the reaction between H_2O_2 and NZVI, protons are consumed (Eq. (4)),[31,32] which can balance the protons generated as a result of hydrolysis of Fe(III). The latter is generated from the rapid oxidation of ferrous species in the presence of H_2O_2, which has been experimentally checked by the no detection of dissolved Fe(II) during that period.

$$Fe^0 + H_2O_2 + 2H^+ \leftrightharpoons Fe^{2+} + 2H_2O \quad (4)$$

Once H_2O_2 was totally consumed and ORP reached again negative values, release of dissolved Fe(II) into solution was observed. Then, the dissolved Fe(II) concentration decreased over reaction time, likely due to adsorption to oxide particles, particularly at high pH value (~8). It is worth noting that the color of suspension changed from black to yellow after the addition of H_2O_2, and gradually turned to black after the 15-h reaction.

Once the ORP and pH values reached steady-state values, a desired concentration of NA was introduced into the reaction system, and residual NA concentration was monitored over time (Figure 1). A slight increase in pH can be mainly attributed to the alkalinity of the NA mother solution, but also to NA binding to oxide surfaces. Indeed,

almost 60% of NA removal was observed after 2 h of reaction time at the working pH (~9). NA removal by, for instance, Fenton-like oxidation is excluded under our experimental conditions, since full mass balance was achieved at the end of reaction, *i.e.* desorbed amounts equivalent to adsorbed ones (Table S1). This great adsorption (~29 µmol per g of initial NZVI added) at an alkaline pH is quite unusual, and thus not comparable with the typical pH-dependence behavior of adsorption of monocarboxylates or polyfunctional compounds, as for example quinolones.[20] Indeed, the sorption behavior of such compounds to metal oxides is generally attributed to a combination of pH-dependent speciation of compound (*e.g.* pK_a of NA = 6.19) and surface charge characteristics of the mineral oxide (PZC of Fe-oxyhyrdoxides is generally between 8 and 9.5).[20] As a result, adsorption is generally high at low pH value and then decreases when pH increases, and becomes negligible at pH higher than 10.[33] Here, the NA adsorption is unusually high at pH around 9, and even increased from 29 to 40 µmol/g when the initial NA concentration increased from 10 to 20 µM, further confirming the high affinity of the NZVI oxidation products toward NA.

3.2. Secondary minerals formation and impacts on NA removal

NZVI can be oxidized and/or transformed into different iron oxides depending on the oxidant dose, which may exhibit contrasting affinities towards NA. For this reason, additional experiments of NZVI oxidation were performed with different H_2O_2 concentrations (Figure S1). Generally, higher H_2O_2 concentration led to a rapid increase

View Article Online
DOI: 10.1039/D0EN00886A

in ORP value in NZVI suspension, and then decrease to reach the initial value, except for the highest H_2O_2 dose. For the sake of clarity, only the last stage, *i.e.* NA adsorption, was shown and the adsorbed amount of NA was plotted versus time for different H_2O_2 concentrations (0 - 10 mM) (Figure 2a). Interestingly, a negligible removal of NA was observed on the fresh NZVI, while the NA removal amount onto the resulting secondary minerals increased with increasing in H_2O_2 dose, yet no significant difference was observed for the two highest doses (5 and 10 mM). It is interesting to note that the NA removal amount by the corrosion particles of NZVI can be enhanced in the presence of humic acid (LHA was used here as model of natural organic matter) (see Figure S3). Indeed, the presence of 5 mg/L of LHA increased the NA adsorbed amount from 22 to 30 µmol/g. This enhanced adsorption in the presence of humic acids can be ascribed to better dispersion of secondary mineral particles, thus increasing available surface area as previously reported.[34]

View Article Online
DOI: 10.1039/D0EN00886A

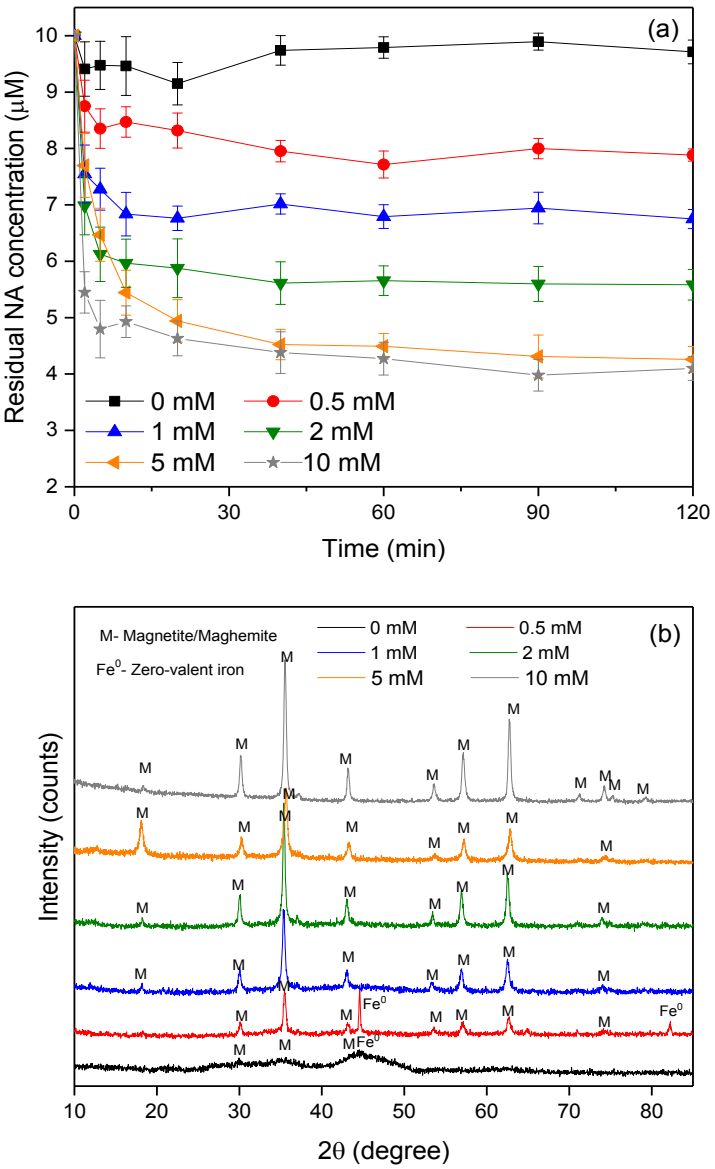

Figure 2. (a) NA removal by the oxidation NZVI samples (b) XRD patterns of secondary minerals at different H_2O_2 concentrations (0 - 10mM); unbuffered systems (pH= 9 ±0.2 for the adsorption stage); [NZVI]=0.2 g·L^{-1}, $[NA]_{initial}$=10 μM, 20 ±1 °C.

As the adsorption capacity is closely related to the properties of iron oxides and hydroxides, the resulting secondary minerals were firstly characterized by XRD (Figure 2b). The XRD pattern of fresh NZVI revealed the presence of a broad peak of α-Fe

View Article Online
DOI: 10.1039/D0EN00886A

(44.5° 2θ) with weak peaks of magnetite and/or maghemite (marked as M) due probably to outer iron oxide shell of NZVI particles.[18] At low H_2O_2 concentration (0.5 mM), peaks of α-Fe were still observed while new peaks corresponding to magnetite and/or maghemite appeared. At H_2O_2 concentration over 1 mM, magnetite/maghemite was detected as the major secondary iron minerals (Figure 2b).

To gain more insight about potential changes in surface properties upon NZVI oxidation, zeta potential and average particle size of the secondary mineral particles were measured. These results showed that H_2O_2 induced oxidation may influence the aggregation behavior in NZVI suspension (Figure S2). While Zeta potential negative value is within the reported values for bare NZVI at alkaline pH (9),[35] H_2O_2 induced oxidation resulted in a significant reduction of the mean size of agglomerates from around 4000 nm to around 800 nm when the H_2O_2 concentration exceeded 2 mM. However, the zeta potential of NZVI suspension did not change significantly over the entire H_2O_2 concentration range. Generally, increasing in negative surface charge of particles may indicate dispersion or lower aggregation.[36] Here, enhancement in the electrostatic repulsion effect and thus the dispersion of the particles is only observed at higher H_2O_2 dose, that could be associated with the formation of magnetite/maghemite particles (Fig. 2b). The high agglomeration observed for the fresh NZVI or slightly oxidized NZVI could be possibly due to electrostatic attractions between various kinds of particles: Fe^0, iron oxides coating the Fe^0 core and other secondary minerals. Furthermore, the van der Waals interactions between these particles may take place

View Article Online
DOI: 10.1039/D0EN00886A

because of the limited electrostatic repulsion between particles. Accordingly, the BET surface area of the oxidized particles (using 5 mM of H_2O_2) (28.2 ± 1.5 m^2/g) was found almost twice higher than the surface area of the fresh NZVI (14.9 ± 1 m^2/g).

Collectively, these results suggest that fresh NZVI (or Fe^0) has negligible affinity for NA adsorption, and the secondary Fe minerals could be responsible of the NA removal in NZVI suspension.

3.3. Structural evolution of NZVI over reaction time

As the highest removal rate of NA was observed with a high dose of H_2O_2 (5 or 10 mM), we have investigated the morphological changes of oxidized NZVI particles over reaction time when 5 mM of H_2O_2 was used for oxidation. Two key stages of NZVI oxidation kinetics were investigated (as shown in Figure 1) : (i) 3h, after H_2O_2 addition and when ORP and pH values have reached a plateau (oxidizing conditions), and (ii) 18h just before NA addition and when ORP and pH values have reached constant values after complete H_2O_2 depletion.

View Article Online
DOI: 10.1039/D0EN00886A

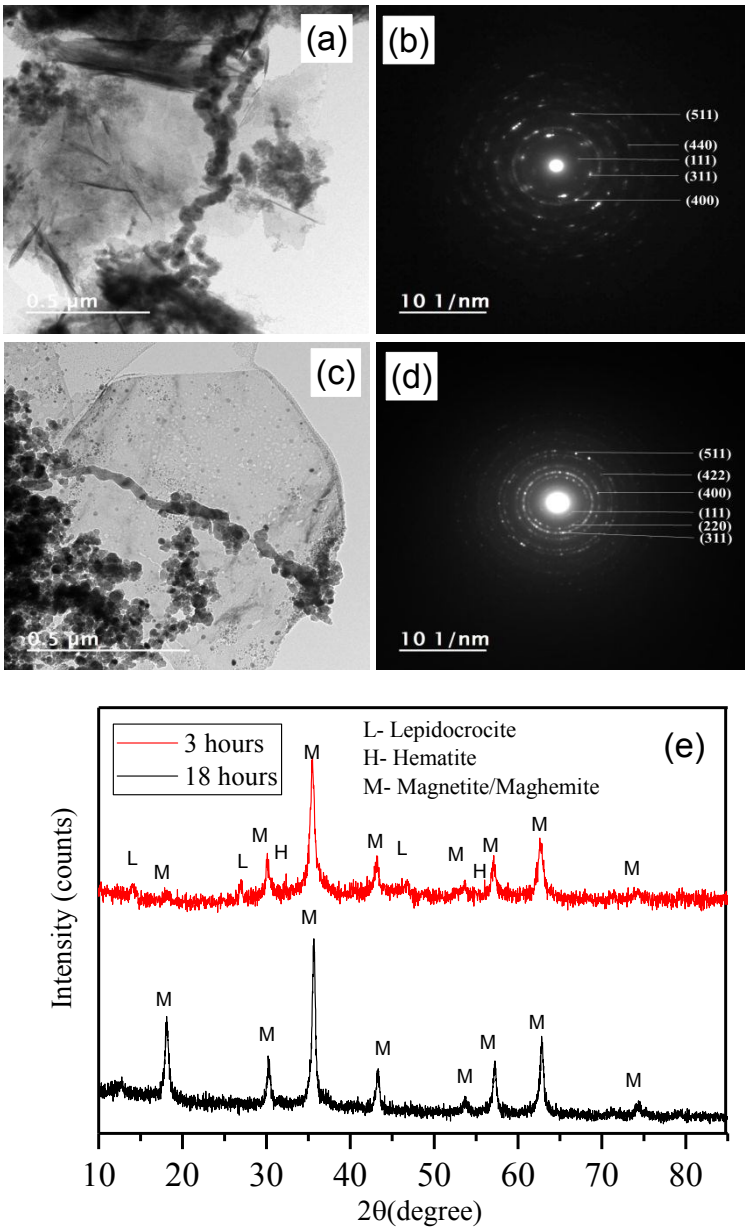

Figure 3. TEM images and SEAD pattern of the oxidized NZVI with 5 mM H_2O_2 at two oxidation times (a and b) 3 hours and (c and d) 18 hours, and (e) corresponding XRD patterns.

In the 3-h sample, we observed the presence of chain-like aggregates of nanoparticles and needle-like shaped individual nanoparticles (Figure 3). The SAED pattern of chain-

like aggregates (Figure 3b) showed the d-spacing of 4.87, 2.53, 2.09, 1.60 and 1.49 Å, which are assigned to the (111), (311), (400), (511), and (440) of magnetite/maghemite phase, respectively.[37] In addition, the XRD of 3-h sample revealed the presence of peaks of magnetite/maghemite, lepidocrocite, and hematite (Figure 3e). This is consistent with previous investigation, which showed that needle-shaped lepidocrocite was formed as a secondary product from NZVI oxidation in oxygenated water.[38] TEM image of 18h oxidized NZVI (Figure 3c) shows the presence of nanoparticles aggregates without other distinct shaped particles. Single nanoparticles (20 nm as an average size) were connected to form chain-like magnetic nanoparticles (see Figure S4). The SAED pattern of these aggregates revealed the reflections of (111, 4.87 Å), (220, 2.98 Å), (311, 2.53 Å), (400, 2.08 Å), (422, 1.70 Å), and (511, 1.59 Å), corresponding to magnetite or maghemite.[39] Though these minerals both have indistinguishable diffraction patterns, the chain-like assembly of these nanoparticles may suggest strong ferromagnetic properties of particles at room temperature. Because the weak dipole–dipole interactions between the maghemite particles are usually not sufficient to result in the chain formation, the chain assemblies observed here tend to support the formation of magnetite as the dominant phase.[40,41] This falls in line with previous report,[42] where magnetite has been detected as the major secondary iron mineral under anoxic conditions (*i.e.* equivalent to conditions here within the 15h-18h period of reaction). In addition, the oxidation of NZVI to magnetite (Fe_3O_4) seems to be more thermodynamically favorable at alkaline pH values.[23,43]

View Article Online
DOI: 10.1039/D0EN00886A

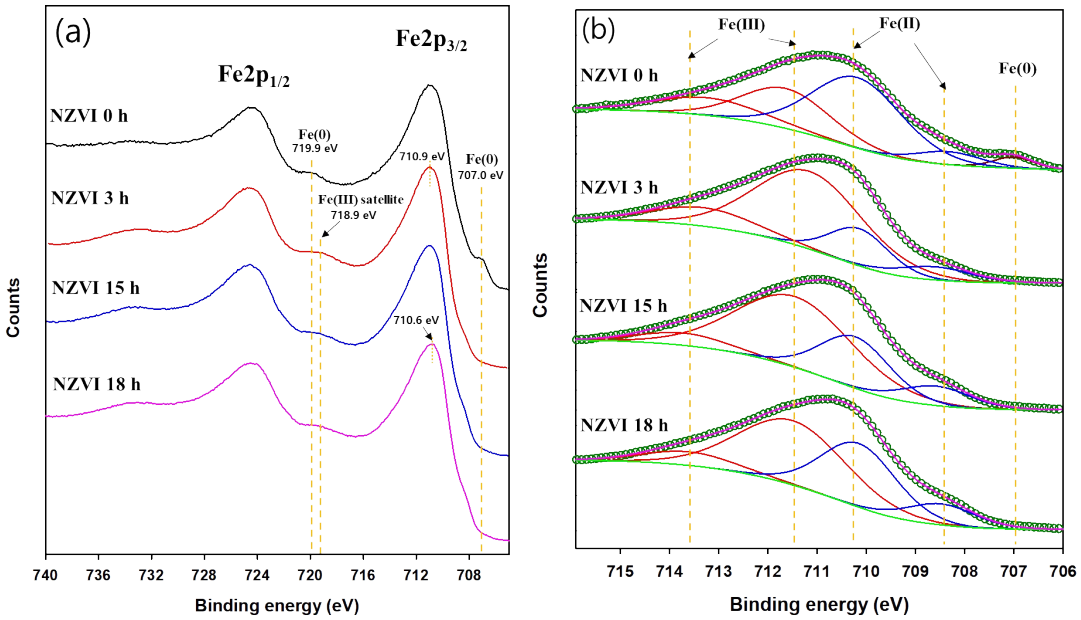

Figure 4. XPS spectra for (a) Fe2p of NZVI before and after reaction with H_2O_2 and (b) and the deconvolution results of $Fe2p_{3/2}$ (706−716 eV). Conditions: $[H_2O_2]$ = 5 mM, [NZVI]=0.2 g·L^{-1}

XPS analyses were conducted on NZVI samples oxidized with 5 mM of H_2O_2 at different reaction times (0, 3, 15 and 18h). The XPS spectra for $Fe2p_{3/2}$ (Figure 4(b)) were composed of five different peaks at 707.0, 708.3−708.5 eV, 710.1−710.3, 711.1−711.6, and 713.2−713.7 eV, which are assigned to the binding energies for Fe(0) (706.5−707.0 eV), Fe(II)-O (708.2−710.9 eV), and Fe(III)-O (711.0–714.0 eV), respectively.[44] In the pristine NZVI, two distinct peaks were observed at 719.9 and 707 eV, corresponding to $Fe2p_{1/2}$ and $Fe2p_{3/2}$ of Fe(0), respectively (Figure 4(a)).[45] After 3-h reaction, we observed the disappearance of Fe(0) peaks and the formation of new Fe(III) satellite peak at 718.9 eV, indicating the presence of Fe(III) minerals (*e.g.* maghemite).[46-48] The proportion of Fe(II) (55.4% → 24.2%) on the NZVI surface

View Article Online
DOI: 10.1039/D0EN00886A

decreased after 3 h-reaction whereas that of Fe(III) increased from 41.2% to 75.8% (Figure 4(b)), underscoring the surface oxidation of NZVI by H_2O_2. However, the Fe(III) satellite peak gradually decreased over reaction time (3 to 18 h), whereas the peak of $Fe2p_{3/2}$ shifted to lower binding energy (710.9 → 710.6 eV) (Figure 4(a)). The disappearance of Fe(III) satellite peak may result from mineral transformation of Fe^{III}-oxides (e.g. maghemite) into magnetite as previously reported.[48] Indeed, the proportion of Fe(II) increased (34.7% at 15 h to 43.3% at 18 h), and Fe(III) decreased (65.3% at 15 h to 56.7% at 18 h) with increasing reaction time (Figure 4b).

Based on all experimental findings above, an oxidation pathway of NZVI by H_2O_2 can be proposed as two successive steps (Figure S5). In the early stage of NZVI oxidation, highly oxidizing condition caused by the addition of a high dose of H_2O_2 can form mixed valence oxides (*i.e.* magnetite), but also Fe^{III}-oxyhydoxides (lepidocrocite, maghemite and hematite), resulting in change of NZVI suspension color from black to yellowish (Figure 1). After the remained H_2O_2 was completely depleted over 15h of reaction time, reducing conditions (ORP value reached the initial value of fresh NZVI suspension) and then release of ferrous ions into solution concurrently take place (Figure 1). Afterwards, the dissolved ferrous ions tend to re-sorb on the surface of Fe(III)-oxyhydroxides at alkaline pH value, leading to their transformation into magnetite as previously reported for lepidocrocite or hematite (Eqs. (5) and (6)).[49,50]

$$2\gamma FeOOH + Fe^{2+} \rightarrow Fe_3O_4 + 2H^+ \quad (5)$$

$$\alpha Fe_2O_3 + Fe^{2+} + H_2O \rightarrow Fe_3O_4 + 2H^+ \quad (6)$$

Color change from yellowish to black of suspension further suggested such transformation into magnetite phase. Therefore, Fe(II)-release during the oxidation of NZVI suspension and its re-adsorption to secondary minerals may influence the surface reactivity of the resulting products.

Additional experiments of NA removal by fresh NZVI or oxidized products (Figure S6) using Good's buffers showed that NA adsorption decreased with pH increasing. However, the NA adsorption at pH 9 was much lower in buffered systems as compared to the un-buffered NZVI suspension (Figure 1). This discrepancy is probably due to the interactions of Good's buffers with the Fe oxide surfaces, which may cause the rapid Fe(0) corrosion and Fe(II) release. [51] It was reported that such Fe(II) release may lead to lepidocrocite formation through Fe(II)-catalyzed transformation of poorly crystallized Fe-oxides (*e.g.* ferrihydrite) and/or oxidation of Fe(II) at acidic-neutral pH.[51] Accordingly, lepidocrocite was identified here as the major phase in buffered NZVI suspension at pH 5.6 and 7 (Figure S7). However, the oxidation products in TRIZMA buffered system (pH 9) were mostly highly amorphous, which makes difficult an accurate identification of secondary iron minerals (Figure S7). It is worth noting that oxidation in TRIZMA buffered system led to dispersion of NZVI particles in suspension and enhancement in zeta potential (Figure S8) compared to that without TRIZMA (Figure S2), thus confirming interactions of TRIZMA molecules with Fe-oxides. Therefore, interactions of organic buffer's molecules with mineral surfaces may

affect the Fe(II) binding. In the absence of Good's buffers, no elution of Fe(II) is expected and thus the surface bound Fe(II) can be preserved. This is consistent with previous works which showed that organic buffers increased the Fe(II) apparent solubility in goethite and magnetite suspensions even in the alkaline pH range.[21-22] Collectively, these results further suggest that the Fe(II) bound to secondary minerals (i.e. magnetite) could control on the surface reactivity and then the binding capacity toward negatively charged contaminants.

3.4. NA adsorption mechanisms on secondary minerals

To check the pH dependence of Fe(II) release and NA sorption onto the NZVI oxidation products, residual concentrations of NA and dissolved Fe(II) in oxidized NZVI suspension were monitored over a wide range of pH (6−11) (Figure 5). NA adsorption was found the greatest between pH 6 and 9, and the lowest between pH 10 and 11. This pH adsorption edges differs from the previously reported data of NA adsorption to Fe-oxyhydroxides[20, 26] or the NA adsorption data obtained here with three synthetic Fe-oxyhydroxides (See Figure S9). Indeed, NA adsorption to non-stoichiometric magnetite (Fe_3O_4)[26], goethite (α-FeOOH)[20] or other ferric oxyhydroxides (maghemite, hematite or lepidocrocite) decreased as increasing pH and became negligible for pH higher than 9. Here, the pH-adsorption curve of NA onto NZVI oxidized products shifts to larger pH values, probably because of the presence of dissolved Fe(II). The concentration of dissolved Fe(II) (no dissolved Fe(III) was found)

View Article Online
DOI: 10.1039/D0EN00886A

decreased as pH increasing. Because of H^+ promoted dissolution of magnetite, Fe(II) dissolution takes place at low pH, which can explain the high amount of dissolved Fe(II) at that pH range.[27] This observation falls in line with a previous investigation on the reactivity assessment of magnetite in presence of variable dissolved Fe(II) amounts [26]. Indeed, it was shown that Fe(II) recharge of magnetite enhanced its binding capacity towards organic and inorganic compounds, shifting the maximum sorption to alkaline pH values.[26] Furthermore, Fe(II)-amendment of non-stoichiometric magnetite (Fe(II)/Fe(III) = 0.40) led to similar sorption capacity as compared to the stoichiometric magnetite (i.e. Fe(II)/Fe(III) = 0.50).[26] In the present work, the Fe(II)/Fe(III) ratio of NZVI oxidized products determined by acid digestion was found very high (1.03) and much more than the expected ratio for a magnetite phase, probably because of the presence of residual traces of Fe^0.

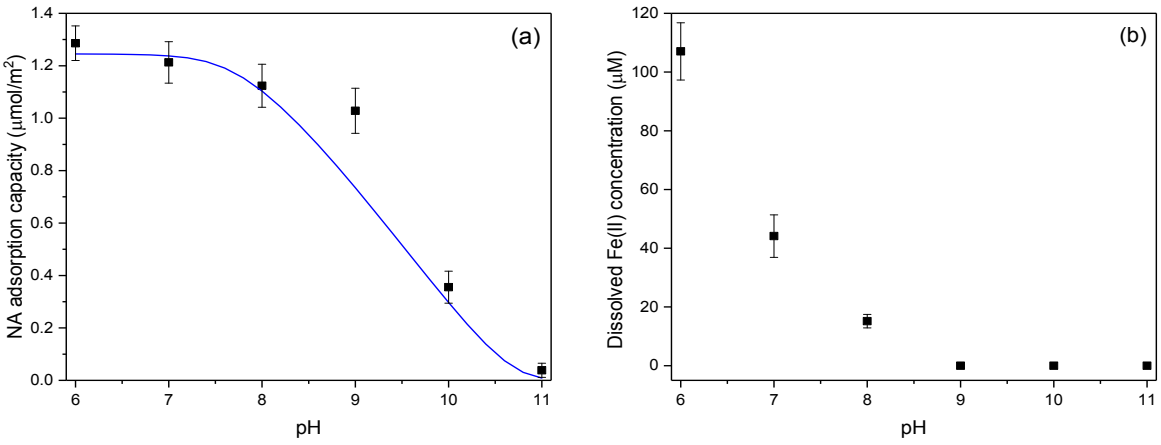

Figure 5. pH-dependency of (a) NA adsorption and (b) dissolved Fe(II) concentration in NZVI suspension after oxidation (5mM H_2O_2). Lines are modeling results. Experimental conditions: [NZVI]= 0.2 g·L^{-1} ,[NA]= 10 µM, 20 ±1 °C. The BET surface area used here is that measured for the oxidized particles (using 5 mM of H_2O_2) (28.2 ± 1.5 m^2/g).

View Article Online
DOI: 10.1039/D0EN00886A

In order to confirm the role of surface bound Fe(II) in the enhanced NA binding, we washed the final NZVI products with DDIW for 3 times and then monitored the NA uptake (Figure S10). Sharp decrease of Fe(II)/Fe(III) ratio from 1.03 to 0.61 upon washing of NZVI products indicated strong loss of Fe(II) during the washing process. For NA adsorption at pH 9 (Figure S10), almost 2-fold decrease in adsorbed amount was observed after the washing process, confirming the crucial role of the surface bound Fe(II) in the enhanced NA adsorption.

As an attempt to explain the enhanced NA adsorption at high pH with respect to the presence of Fe(II), we used a surface complexation model, previously developed for the stoichiometric magnetite.[26] We assumed that NA binds to two surface hydroxo groups[20, 52] by involving its carboxylate and its keto-group as following:

$$2 \equiv FeOH + 2\ H^+ + NA^- \rightleftharpoons (\equiv Fe)_2NA^+ + 2\ H_2O \qquad {}^{S}K \qquad (7)$$

As presented in Figure 5, accurate description of experimental results of NA adsorption by the oxidized NZVI particles was obtained at a wide pH range (6−11). We used the measured dissolved Fe(II) concentration at the end of each adsorption experiment as input parameters to account for NA−Fe(II) aqueous complex formation. The good accuracy with the experimental data using the modeling parameters of the stoichiometric magnetite (see Table S2) suggests that magnetite controls NA binding to oxidized NZVI, and further confirms the key role of surface bound Fe(II).

It is interesting to note that the great binding capacity of the corrosion particles of NZVI at alkaline pH values also concerns other antibiotics of contrasting structure and properties. Indeed, great adsorption of TET (*i.e.* 70% removal of 10µM) onto the oxidized NZVI particles was observed at pH 9.0 ± 0.2 (Figure S11). Taken together, these results highlight the key role of Fe(II) generated along the NZVI oxidation process in promoting greater binding abilities of the secondary minerals.

4. Conclusions

NZVI oxidation or passivation in ambient environments can lead to either formation of Fe^{II}-bearing phases on the NZVI surface or complete oxidation to ferric (oxyhydr)oxides. Under the experimental conditions of this study, NZVI oxidation led to formation of Fe^{II}-bearing secondary minerals, with magnetite as the major phase. The latter exhibited higher adsorption ability for organic contaminants, in contrast to the fresh NZVI. In addition, an unexpected great adsorption at alkaline pH values was observed with the formed secondary Fe minerals. This behavior is due to the gradual increase in Fe(II) content at the surface of magnetite phase over the reaction time. A surface complexation model confirmed that NA adsorption onto the secondary magnetite is due to the formation of surface bound Fe(II). If Fe(II) is released into solution, the surface bound Fe(II) decreased together with the NA adsorbed amount at alkaline pH values. As iron (oxyhydr)oxide-coated NZVI particles or Fe(II)-Fe(III)

View Article Online
DOI: 10.1039/D0EN00886A

(oxyhydr)oxides may exhibit different adsorption affinities toward negatively charged molecules (e.g. antibiotics) or positively charged compounds, more attention should be paid to the reactivity assessment of passivated NZVI particles or corrosion products. Therefore, the modeling of contaminant fate and transport should consider the impact of these secondary Fe minerals on the mobility of emerging contaminants in soil and groundwater.

Conflicts of interest

There are no conflicts to declare.

Acknowledgements

We acknowledge support from the National Research Foundation of Korea (project no. NRF- NRF-2019R1C1C1003316). We gratefully acknowledge to Isabelle Soutrel (LC/UV) and Vincent Dorcet (THEMIS platform) for the assistance.

Supplementary information: Additional information regarding oxidation and adsorption kinetics, TEM images and XRD data, additional data on zeta potential and average particle size measurements, and surface complexation model parameters.

References

1. S. H. Joo, A. J. Feitz and T. D. Waite, Oxidative Degradation of the Carbothioate Herbicide, Molinate, Using Nanoscale Zero-Valent Iron. *Environ. Sci. Technol.,* 2004, ***38***, 2242-2247.
2. J. Ma, D. He, R. N. Collins, C. He and T. D. Waite, The tortoise versus the hare - Possible advantages of microparticulate zerovalent iron (mZVI) over nanoparticulate zerovalent iron (nZVI) in aerobic degradation of contaminants, *Water Res.*, 2016, **105**, 331-340.
3. S. Tsarev, R. N. Collins, E. S. Ilton, A. Fahy and T. D. Waite, The short-term reduction of uranium by nanoscale zero-valent iron (nZVI): role of oxide shell, reduction mechanism and the formation of U(V)-carbonate phases, *Environ. Sci. Nano*, 2017, **4**, 1304-1313.
4. D. He, J. Ma, R. N. Collins and T. D. Waite, Effect of Structural Transformation of Nanoparticulate Zero-Valent Iron on Generation of Reactive Oxygen Species, *Environ. Sci. Technol.,* 2016, **50**, 3820-3828.
5. T. Liu, X. Li and T. D. Waite, Depassivation of Aged Fe0 by Ferrous Ions: Implications to Contaminant Degradation, *Environ. Sci. Technol.*, 2013, **47**, 13712-13720.
6. T. Phenrat, T. Thongboot and G. V. Lowry, Electromagnetic Induction of Zerovalent Iron (ZVI) Powder and Nanoscale Zerovalent Iron (NZVI) Particles Enhances Dechlorination of Trichloroethylene in Contaminated Groundwater and Soil: Proof of Concept. *Environ. Sci. Technol.,* 2016, **50**, 872-880.
7. Y.-T. Wei, S.-C. Wu, C.-M. Chou, C.-H. Che, S.-M. Tsai and H.-L. Lien, Influence of nanoscale zero-valent iron on geochemical properties of groundwater and vinyl chloride degradation: A field case study, *Water Res.,* 2010, **44**, 131-140.
8. C. Su, R.W Pulsa, T. A. Krug, M. T. Watling, S. K. O'Hara, S. K; J. W. Quinnc and N. E. Ruiz, Travel distance and transformation of injected emulsified zerovalent iron nanoparticles in the subsurface during two and half years, *Water Res.*, **47**, 4095-4106.
9. W. X. Zhang, Nanoscale Iron Particles for Environmental Remediation: An Overview. *J. Nanopart. Res*. 2003, **5**, 323-332.
10. B. C. Reinsch, B. Forsberg, R. L. Penn, C. S. Kim and G. V. Lowry, Chemical Transformations during Aging of Zerovalent Iron Nanoparticles in the Presence of Common Groundwater Dissolved Constituents, *Environ. Sci. Technol.*, 2010, 44, 3455-3461.
11. J.-Y. Ahn, C. Kim, H.-S. Kim, K.-Y. Hwang and I. Hwang, Effects of oxidants on in situ treatment of a DNAPL source by nanoscale zero-valent iron: A field study, *Water Res.*, 2016, **107**, 57-65.
12. J. Chen, Z. Xiu, G. V. Lowry and P. J. J. Alvarez, Effect of natural organic matter on toxicity and reactivity of nano-scale zero-valent iron, *Water Res.*, 2011, **45**,

1995-2001.

13. H. Pullin, R. A. Crane, D. J. Morgan and T. B. Scott, The effect of common groundwater anions on the aqueous corrosion of zero-valent iron nanoparticles and associated removal of aqueous copper and zinc, *J. Environ. Chem. Eng*, 2017, **5**, 1166-1173.
14. A. Liu, J. Liu, J. Han and W.-x. Zhang, Evolution of nanoscale zero-valent iron (nZVI) in water: Microscopic and spectroscopic evidence on the formation of nano- and micro-structured iron oxides, *J. Hazard. Mater.*, 2017, **322**, 129-135.
15. C. Poppe, M. Ayroud, G. Ollis, M. Chirino-Trejo, N. Smart, S. Quessy and P. Michel, Trends in Antimicrobial Resistance of Salmonella Isolated from Animals, Foods of Animal Origin, and the Environment of Animal Production in Canada, 1994-1997, *Microb. Drug Resist*, 2001, **7**, 197-212.
16. F. Campioni, R. A. Souza, V. V. Martins, E. G. Stehling, A. M. M. Bergamini and J. P. Falcão, Prevalence of gyrA Mutations in Nalidixic Acid-Resistant Strains of Salmonella Enteritidis Isolated from Humans, Food, Chickens, and the Farm Environment in Brazil, *Microb. Drug Resist.*, 2016, **23**, 421-428.
17. U. Schwertmann, R. M. Cornell, Iron Oxides in the Laboratory: Preparation and Characterization. Wiley- VCH: New York, 2000.
18. S. Bae, S. Gim, H. Kim and K. Hanna, Effect of $NaBH_4$ on properties of nanoscale zero-valent iron and its catalytic activity for reduction of p -nitrophenol, *Appl. Catal., B*, 2016, **182**, 541-549
19. S. Bae and W. Lee, Influence of Riboflavin on Nanoscale Zero-Valent Iron Reactivity during the Degradation of Carbon Tetrachloride, *Environ. Sci. Technol.*, 2014, **48**, 2368-2376.
20. J. Xu, R. Marsac, C. Wei, F. Wu, J. F. Boily and K. Hanna, Cobinding of Pharmaceutical Compounds at Mineral Surfaces: Mechanistic Modeling of Binding and Cobinding of Nalidixic Acid and Niflumic Acid at Goethite Surfaces, *Environ. Sci. Technol.*, 2017, **51**, 11617-11624.
21. A. Buchholz, C. Laskov and S. B. Haderlein, Effects of Zwitterionic Buffers on Sorption of Ferrous Iron at Goethite and Its Oxidation by CCl_4, *Environ. Sci. Technol.*, 2011, **45**, 3355-3360.
22. R. Marsac, M. Pasturel and K. Hann, Reduction Kinetics of Nitroaromatic Compounds by Titanium-Substituted Magnetite, *J. Phys. Chem. C,* 2017, **121**, 11399-11406.
23. D. L. Parkhurst and C. A. J. Appelo, User's guide to PHREEQC (Version 2): A computer program for speciation, batch-reaction, one-dimensional transport, and inverse geochemical calculations, *Water Resources Investigations Report*, 1999, 99-4259,
24. W. R. Vincent, S. G. Schulman, J. M. Midgley, W. J. van Oort and R. H. A. Sorel, Prototropic and metal complexation equilibria of nalidixic acid in the physiological pH region, Int. J. Pharm., 1981, **9**, 191-198.

25. R. Jolsterå, L. Gunneriusson and A. Holmgren, Surface complexation modeling of Fe_3O_4-H^+ and Mg(II) sorption onto maghemite and magnetite, *J. Colloid Interface Sci.*, 2012, **386**, 260-267.
26. W. Cheng, R. Marsac and K. Hanna, Influence of Magnetite Stoichiometry on the Binding of Emerging Organic Contaminants, *Environ. Sci. Technol.*, 2018, **52**, 467-473.
27. S. Bae and K. Hanna, Reactivity of Nanoscale Zero-Valent Iron in Unbuffered Systems: Effect of pH and Fe(II) Dissolution, *Environ. Sci. Technol.*, 2015, **49**, 10536-10543.
28. Y.-H. Bai, Y. Du, J.-J. Xu and H.-Y. Chen, Choline biosensors based on a bi-electrocatalytic property of MnO_2 nanoparticles modified electrodes to H_2O_2, Electrochem. Commun., 2007, **9**, 2611-2616.
29. T. A. Kurniawan and W.-h. Lo, Removal of refractory compounds from stabilized landfill leachate using an integrated H_2O_2 oxidation and granular activated carbon (GAC) adsorption treatment, *Water Res.*, 2009, **43**, 4079-4091.
30. N. V. Klassen, D. Marchington and H. C. E. McGowan, H_2O_2 Determination by the I3- Method and by $KMnO_4$ Titration, *Anal. Chem.*, 1994, **66**, 2921-2925.
31. Y. Segura, F. Martínez, J. A. Melero and J. L. G. Fierro, Zero valent iron (ZVI) mediated Fenton degradation of industrial wastewater: Treatment performance and characterization of final composites, Chem. Eng. J., 2015, **269**, 298-305.
32. W. Zhang, H. Gao, J. He, Y. Peng and X. Xu, Removal of norfloxacin using coupled synthesized nanoscale zero-valent iron (nZVI) with H_2O_2 system: Optimization of operating conditions and degradation pathway, *Sep. Purif. Technol.*, 2016, **172**, 158-167.
33. W. Cheng, E. L. Kalahroodi, R. Marsac and K. Hanna, Adsorption of Quinolone Antibiotics to Goethite under Seawater Conditions: Application of a Surface Complexation Model, *Environ. Sci. Technol.*, 2019, **53**, 1130-1138.
34. Q. Du, G. Li, S. Zhang, J. Song, Y. zhao and F. Yang, High-dispersion zero-valent iron particles stabilized by artificial humic acid for lead ion removal, *J. Hazard. Mater.*, 2020, **383**, 121170.
35. H. M. Ibrahim, M. Awad, A. S. Al-Farraj and A. M. Al-Turki, Stability and Dynamic Aggregation of Bare and Stabilized Zero-Valent Iron Nanoparticles under Variable Solution Chemistry, *Nanomaterials*, 2020, **10**, 192.
36. H. Dong and I. M. C. Lo, Influence of humic acid on the colloidal stability of surface-modified nano zero-valent iron, *Water Res.*, 2013, **47**, 419-427.
37. E. S. Krystofiak, E. C. Mattson, P. M. Voyles, C. J. Hirschmugl, R. M. Albrecht, M. Gajdardziska-Josifovska and J. A. Oliver, Multiple Morphologies of Gold–Magnetite Heterostructure Nanoparticles are Effectively Functionalized with Protein for Cell Targeting, *Microsc. Microanal.*, 2013, **19**, 821-834.
38. A. Liu, J. Liu, B. Pan and W.-x. Zhang, Formation of lepidocrocite (γ-FeOOH) from oxidation of nanoscale zero-valent iron (nZVI) in oxygenated water, *RSC*

Adv., 2014, **4**, 57377-57382.

39. R. P. Araújo-Neto, E. L. Silva-Freitas, J. F. Carvalho, T. R. F. Pontes, K. L. Silva, I. H. M. Damasceno, E. S. T. Egito, A. L. Dantas, M. A. Morales and A. S. Carriço, Monodisperse sodium oleate coated magnetite high susceptibility nanoparticles for hyperthermia applications, *J. Magn. Magn. Mater.*, 2014, **364**, 72-79.
40. Y. Lalatonne, J. Richardi and M. P. Pileni, Van der Waals versus dipolar forces controlling mesoscopic organizations of magnetic nanocrystals, *Nat. Mater.*, 2004, **3**, 121-125.
41. M. I. Dar and S. A. Shivashankar, Single crystalline magnetite, maghemite, and hematite nanoparticles with rich coercivity, *RSC Adv.*, 2013, **4**, 4105-4113.
42. S. Bae, R. N. Collins, T. D. Waite and K. Hanna, Advances in Surface Passivation of Nanoscale Zerovalent Iron: A Critical Review, *Environ. Sci. Technol.*, 2018, **52**, 12010-12025.
43. Y. Liu and G. V. Lowry, Effect of particle age (Fe^0 content) and solution pH on NZVI reactivity: H2 evolution and TCE dechlorination, *Environ. Sci. Technol.*, 2006, **40**, 6085-6090.
44. M. A. Kumar, S. Bae, S. Han, Y. Chang and W. Lee, Reductive dechlorination of trichloroethylene by polyvinylpyrrolidone stabilized nanoscale zerovalent iron particles with Ni, *J. Hazard. Mater.*, 2017, **340**, 399-406.
45. S. Luo, T. Lu, L. Peng, J. Shao, Q. Zeng and J.-D. Gu, Synthesis of nanoscale zero-valent iron immobilized in alginate microcapsules for removal of Pb(II) from aqueous solution, *J. Mater. Chem. A,* 2014, **2**, 15463-15472.
46. T. Yamashita and P. Hayes, Analysis of XPS spectra of Fe^{2+} and Fe^{3+} ions in oxide materials, *Appl. Surf. Sci.*, 2008, **254**, 2441-2449.
47. T. Radu, C. Iacovita, D. Benea and R. Turcu, X-Ray Photoelectron Spectroscopic Characterization of Iron Oxide Nanoparticles, *A Appl. Surf. Sci.,* 2017, **405**, 337-343.
48. F. Kraushofer, Z. Jakub, M. Bichler, J. Hulva, P. Drmota, M. Weinold, M. Schmid, M. Setvin, U. Diebold, P. Blaha and G. S. Parkinson, Atomic-Scale Structure of the Hematite α-Fe2O3(1$\bar{1}$02) "R-Cut" Surface, *J. Phys. Chem. C*, 2018, **122**, 1657-1669.
49. M. Usman, M. Abdelmoula, K. Hanna, B. Grégoire, P. Faure and C. Ruby, Fe^{II} induced mineralogical transformations of ferric oxyhydroxides into magnetite of variable stoichiometry and morphology, *J. Solid State Chem.*, 2012, **194**, 328-335.
50. J. P. Jolivet and E. Tronc, Interfacial electron transfer in colloidal spinel iron oxide. Conversion of Fe_3O_4-γFe_2O_3 in aqueous medium, *J. Colloid Interface Sci.*, 1988, **125**, 688-701.
51. C. He, D. He, R. N. Collins, S. Garg, Y. Mu and T. D. Waite, Effects of Good's Buffers and pH on the Structural Transformation of Zero Valent Iron and the Oxidative Degradation of Contaminants, *Environ. Sci. Technol.*, 2018, **52**, 1393-1403.

52. R. Marsac, S. Martin, J.-F. Boily and K. Hanna, Oxolinic Acid Binding at Goethite and Akaganéite Surfaces: Experimental Study and Modeling, *Environ. Sci. Technol.*, 2016, **50**, 660-668.

View Article Online
DOI: 10.1039/D0EN00886A

TOC

Surface bound Fe(II) on the NZVI secondary minerals would affect the fate and mobility of quinolones antibiotics in the environment.